The Effect of Controller Design on Delayed Bilateral Teleoperation Performance: An Experimental Comparison

Ruud Beerens, Dennis Heck, Alessandro Saccon, and Henk Nijmeijer, *Fellow, IEEE*

***Abstract*— This paper presents a detailed experimental comparison of control architectures for delayed bilateral teleoperation. The main goal is to illustrate the key differences in controller performance that can be expected in practice, independent of the human operator, as a function of the communication delay. Existing architectures can be divided into bilateral motion synchronization, where the master and slave controllers implement an as-stiff-as-possible coupling between the master and slave devices, and direct force-reflecting architectures, where the slave controller mimics the operator action, and the master controller reflects the slave-environment interaction forces. Six architectures are analyzed using standard performance indices to assess motion tracking, force reflection, and stiffness reflection quality. In addition, the architectures are also compared on physical operator effort, which is a newly introduced metric to quantify the required operator's effort to execute free motion tasks. The results illustrate that, for increasing delays, direct force-reflecting architectures (in particular, a position/force-force architecture) are superior to bilateral motion synchronizing controllers, in the sense that they are the least sensitive to delays. In contrast, all bilateral motion synchronizing architectures significantly suffer from a reduction in motion tracking or stiffness reflection, or an increased operator effort, when the delay increases. While these conclusions are drawn on a one-degree-of-freedom (DOF) setup, we expect these trends to maintain valid in general, and therefore, the authors suggest that future controller designs for delayed bilateral teleoperation should explore direct force-reflecting architectures more extensively to achieve better performance.**

***Index Terms*— Delay systems, performance evaluation, telerobotics.**

I. Introduction

MANY different control architectures for bilateral teleoperation with communication delays have been proposed over the past 30 years (see [1], [2], and references therein).

Manuscript received January 30, 2019; revised May 9, 2019; accepted June 3, 2019. Date of publication July 3, 2019; date of current version August 6, 2020. Manuscript received in final form June 13, 2019. This work is part of the research programme H-Haptics (project number 12157) and CHAMeleon (project number 13896), which are (partly) financed by the Netherlands Organisation for Scientific Research (NWO). Recommended by Associate Editor A. Chakrabortty. *(Corresponding author: Ruud Beerens.)*

R. Beerens, A. Saccon, and H. Nijmeijer are with the Dynamics and Control Group, Department of Mechanical Engineering, Eindhoven University of Technology, 5600 MB Eindhoven, The Netherlands (e-mail: r.beerens@tue.nl; a.saccon@tue.nl; h.nijmeijer@tue.nl).

D. Heck is with ASML, De Run 6501, 5504DR Veldhoven, The Netherlands (e-mail: dennis.heck@asml.com).

Color versions of one or more of the figures in this article are available online at http://ieeexplore.ieee.org.

Digital Object Identifier 10.1109/TCST.2019.2923703

Communication delays highly affect both the closed-loop stability and performance of the teleoperator, often measured in terms of motion synchronization and accurate rendering of the slave-environment interaction force to the operator. One of the first papers investigating this phenomenon is [3]. When designing a high-performance teleoperator (for example, robotically assisted surgery [4], remotely operated construction work [5], or remote maintenance in future nuclear fusion reactors [6]), it is highly important to understand how the performance is affected by the delays. Despite several (scattered) theoretical and experimental studies, a clear performance comparison of different control strategies, as a function of the delay, is still missing in the literature. The main purpose of this paper is, therefore, to start creating such an understanding by illustrating the key differences in controller performance that can be expected in practice. To this end, we present an experimental comparison analysis of the performance, as a function of the communication delay and independent of the human operator.

Control architectures for bilateral teleoperation can be classified based on their primary design philosophy, namely bilateral motion synchronization or direct force-reflection (see Fig. 1). In bilateral motion synchronization, both the master and slave controllers aim at motion synchronization. The slave-environment interaction force is reflected indirectly by creating an as-tight-as-possible coupling between the master and the slave, typically using a virtual spring and damper. A well-known example of this type of scheme is the position–position (P-P) architecture (see [7]). In direct force-reflection, the slave controller acts as a virtual operator, mimicking the motion of the master on the slave. The master controller acts as a virtual environment, reflecting the slave-environment interaction force obtained by direct measurements. An example of this class of controllers is the position–force (P-F) architecture (see [8], [9]).

The effect of communication delays on both stability and performance is different for architectures designed according to either of these philosophies. For bilateral motion synchronization, the delay typically affects the stability during the free motion phase and manifests itself by an out-of-phase oscillation of the master and slave devices, with increasing amplitude. Stability can be guaranteed by using scattering [11], wave variables [12] (at the cost of losing asymptotic position tracking properties), or damping injection [2]. From a performance point of view, the lags between the master and slave position

1063-6536 © 2019 IEEE. Personal use is permitted, but republication/redistribution requires IEEE permission.
See https://www.ieee.org/publications/rights/index.html for more information.

Authorized licensed use limited to: ASML Netherlands B.V.. Downloaded on August 07,2020 at 07:40:17 UTC from IEEE Xplore. Restrictions apply.

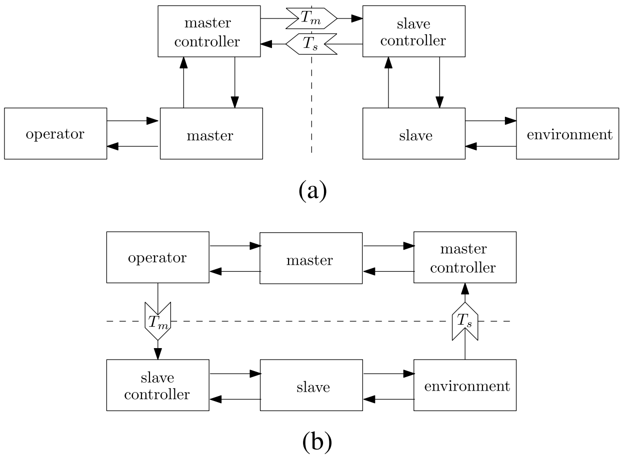

Fig. 1. Block diagrams of two classes of control approaches [10]. Arrows represent information flows, and T_m and T_s denote master–slave communication delays. (a) Bilateral motion synchronization. (b) Direct force-reflection.

movements can cause large reaction forces (also known as delay-induced forces; see [10] and Remark 1) that are heavily felt by the operator. These forces are caused by the motion feedback terms in the master controller, counteracting the operator's movement, and make the system feel heavier to the operator [8].

For direct force-reflection, the teleoperator is unilateral in free motion, and therefore, stability is not affected by delays in this phase. Furthermore, direct force-reflection architectures do not suffer from delay-induced forces since only the slave-environment interaction force is reflected, and no motion feedback terms are present in the master controller. However, these architectures are known to have severe stability issues when the slave makes contact with stiff environments. This instability is sometimes caused by the unstable dynamics of the teleoperator in the contact phase, but mostly due to the switching dynamics resulting from the slave making or breaking contact with the environment (see [8], [13]). Especially in the presence of delays, the operator may not be able to bring and keep the slave in contact with the environment. Typically, the master recoils violently, dragging the slave along with it [14]. Stable slave-environment interaction can be achieved by, e.g., damping injection, as will be illustrated in Sections III and IV.

For increasing values of the delays, the amount and kind of performance loss are different for each control architecture. A good understanding of how the performance is affected by the delays is, therefore, a key when designing high-performance controllers for bilateral teleoperation. In the literature, few studies provide a comparison of architectures using *ad hoc* performance criteria designed to quantitatively capture several aspects of performance. However, to the best of the authors' knowledge, an extensive experimental comparison of both bilateral motion synchronization and direct force-reflection architectures, as a function of the communication delay, has not yet been presented. The purpose of this paper is to start filling this gap.

In [8], Lawrence analytically compared several architectures. It is concluded that, for the delay-free case, the well-known four-channel controller provides the best performance "in the sense of accurate transmission of task impedances to the operator". Independently, the same conclusion is drawn in [15]. In [16], an analysis is presented in which the effect of communication delays is investigated. Several two-channel architectures are compared analytically with the four-channel controller on the transmittable range of impedances. It is concluded that the two-channel architectures suffer less from a performance degradation for increasing delays than a four-channel controller, but the use of both position and force information yields the best performance. In [17], ten different controllers are compared on motion tracking, perceived inertia, and damping in free motion, and reflected stiffness and position drift in the contact phase. Each architecture was thoroughly analyzed, both analytically and in simulation, but the authors did not arrive at a specific conclusion.

A general drawback of these analytical studies is that they do not include practical limitations, such as measurement noise, limited encoder resolution, sampling time, and drive-train imperfections (e.g., friction and compliance). These limitations also affect the performance that can be achieved in practice and should, therefore, be included in the analysis, as done in [18]–[21]. In [21], it is illustrated that, in a palpation task with soft tissue, the P-F architecture yields a better sensitivity of the transmitted impedance to the changes in the environment than a P-P controller. In [18], the P-P, P-F, and four-channel architectures are compared, where the four-channel controller performs best in terms of free motion position tracking, impedance reflection, and force tracking, thereby confirming Lawrence's analytical results. Unfortunately, delays are not included in these analyses. Communication delays are instead considered in [19], where the force data are explored in a wave variables setting. The authors conclude that the use of force data improves the performance of the teleoperator, compared with the classical wave variables scheme, in the presence of delays. Rodríguez-Seda *et al.* [20] use 18 subjects to analyze the effect of data loss on the stability, force reflection accuracy, and stiffness perception for both constant and time-varying delays. They conclude that the loss of data is less critical compared with the effect of time delays. However, only bilateral motion synchronizing architectures (mainly using wave variables) are analyzed, and the architectures that use force information explicitly are not included.

In this paper, six control architectures are reviewed and compared experimentally on a variety of performance metrics using a rotational one-degree-of-freedom (DOF) setup. The selected architectures cover both bilateral motion synchronization and direct force-reflecting architectures, thus representing a broad range of existing controllers. The main contribution of this paper is an illustration of the key differences in achievable performance between the controllers for specific bilateral teleoperation tasks, as a function of the communication delay and independent of the human operator, by means of an experimental comparison study. The results illustrate the key differences in controller behavior and the inherent performance degradation in order to warrant stability as the delay increases, which can help designers to select a suitable architecture.

Authorized licensed use limited to: ASML Netherlands B.V.. Downloaded on August 07,2020 at 07:40:17 UTC from IEEE Xplore. Restrictions apply.

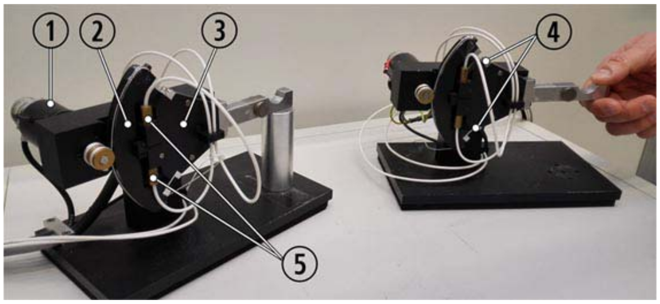

Fig. 2. One-DOF experimental teleoperation setup. An operator interacts with the master device (right), while the slave (left) interacts with a stiff environment (the aluminum cylinder).

The second contribution is the design of a new metric that describes the operator's effort required to operate the system. The third contribution is the adaptation of existing motion tracking, force reflection, and stiffness reflection metrics in such a way that the communication delays are suitably considered. The controller performance is analyzed experimentally for the free motion and contact phases considered separately, similar to the above-mentioned studies.

This paper is organized as follows. Section II introduces the one-DOF setup employed in our comparison study, and Section III covers the considered control architectures. Section IV presents the experimental design and performance metrics used in the analysis. The results are presented and analyzed in Section V, and a discussion follows in Section VI. A conclusion is presented in Section VII.

Notation: Throughout this paper, positions and forces are used in a broader sense. Since the setup in this paper consists of two devices with one revolute joint, these quantities should be interpreted as rotations and torques. The subscripts $i \in \{m, s\}$ and $j \in \{m, s\}$, $j \neq i$, denote either the master (m) or slave (s) device. The value of the communication delay from master to slave is denoted by T_m and from slave to master by T_s. For the sake of clarity, the time argument of all functions in the controllers will be omitted: in particular, we will use q_i and $q_i^{T_i}$ to denote, respectively, $q_i(t)$ and its delayed version $q_i(t - T_i)$.

II. Experimental One-DOF Setup

The experimental setup consists of a revolute master and slave device, as shown in Fig. 2. Each device is actuated by a Maxon RE35 dc servo motor ①, driving a segment to which the end-effector is attached via a Capstan transmission [22]. The rotational segment is split into two concentric parts, ② and ③, connected by two leaf springs ④. The springs have a nominal torsional stiffness of $3.5 \cdot 10^3$ Nm/rad [22]. The applied torque is measured indirectly using two inductive sensors ⑤ that measure the relative rotation between the inner and outer segments. The resolution of the torque measurements is $5.25 \cdot 10^{-4}$ Nm. All experiments are sampled at 2 kHz. The position measurements are filtered with the first-order low-pass filter with a cutoff frequency of 80 Hz. Velocity signals are obtained by numerically differentiating the filtered position signals. The torque measurements are filtered with the first-order low-pass filter with a cutoff frequency of 30 Hz.

Based on a system identification procedure performed in [22] and [23], the master and slave dynamics can be described by the following mass-damper system:

$$m_m \ddot{q}_m + b_m \dot{q}_m = \tau_{mc} + \tau_h \tag{1a}$$

$$m_s \ddot{q}_s + b_s \dot{q}_s = \tau_{sc} - \tau_e \tag{1b}$$

with inertia parameters $m_m = 2 \cdot 10^{-3}$ kgm^2 and $m_s = 2.2 \cdot 10^{-3}$ kgm^2, and damping parameters $b_m = 5 \cdot 10^{-3}$ Nms/rad and $b_s = 7 \cdot 10^{-3}$ Nms/rad. Moreover, τ_{ic} denotes the control torque, τ_h denotes the torque the operator exerts on the master device, and τ_e denotes the slave-environment interaction torque.

III. Control Architectures

Of the six architectures considered in this paper, four can be classified as bilateral motion synchronization (PDd, W, WT, and 4C), and two architectures are direct force-reflection controllers (P-F and PF-F). These architectures are introduced below.

A. Proportional–Derivative + damping control (PDd)

In the bilateral motion synchronizing PD+damping architecture (see [2]), the bilateral coupling between master and slave is achieved via proportional and derivative terms. The master and slave controllers are given by

$$\tau_{ic} = K_{pi}\left(q_j^{T_j} - q_i\right) + K_{di}\left(\dot{q}_j^{T_j} - \dot{q}_i\right) - B_i \dot{q}_i \tag{2}$$

where K_{pi} denotes the proportional control gain, K_{di} denotes the derivative control gain, and B_i denotes the local damping gain. An analysis provided in [2], [24], and [25], employing Lyapunov-like functionals, suggests that the stability of the teleoperator is guaranteed if the controller parameters satisfy the inequality

$$4 B_m B_s > K_{pm} K_{ps}\left(T_m^2 + T_s^2\right). \tag{3}$$

Tuning the proportional gains K_{pi} is subject to a performance tradeoff. For good force reflection, a stiff connection between master and slave is required. For the PDd architecture, this requires high values for K_{pi}. However, it follows from (3) that, in order to guarantee stability, high proportional gains imply the requirement of high values for the damping gains B_i. Damping injection contributes to a sluggish response that operators find unsatisfactory [13], and the impact of the slave with the environment is perceived softer than without damping [26]. Moreover, the delay-induced forces increase with an increasing value for K_{pm} (see Remark 1 below) that negatively influences the teleoperator performance.

Remark 1: Delay-induced forces are additional forces resulting from the delays and implemented by the master controller. These forces are not related to the slave-environment interaction and could, therefore, be misleading for the operator. Focusing only on the proportional term of (2), we obtain, after rewriting

$$\begin{aligned} \tau_{mc} &= K_{pm}\left(q_s^{T_s} - q_m\right) && \text{(4a)} \\ &= K_{pm}(q_s - q_m) + K_{pm}\left(q_s^{T_s} - q_s\right) && \text{(4b)} \end{aligned}$$

Authorized licensed use limited to: ASML Netherlands B.V.. Downloaded on August 07,2020 at 07:40:17 UTC from IEEE Xplore. Restrictions apply.

where the last term on the right-hand side of (4b) represents the delay-induced force contribution. These forces increase with faster movements, a larger value of K_{pm}, and a larger value of the communication delay. The operator has to overcome the delay-induced forces by exerting more force on the master device to achieve the same motion, compared with the delay-free case, or to the controllers without delay-induced forces.

B. Wave Variables (W)

Based on the results of transmission line theory, Anderson and Spong [11] introduced the *scattering transformation* to create a passive (lossless) communication channel. Niemeyer and Slotine [7] presented an equivalent formulation based on *wave variables*, which encodes velocity and force information of the devices. Only the wave variables are then transmitted between the master and the slave. Subsequent to their introduction, many wave variable architectures have been proposed in the literature. Here, the original symmetric architecture with impedance matching, to eliminate *wave reflections* [12], is considered, i.e.,

$$\tau_{ic} = K_{pi} \int_0^t (\dot{q}_{id} - \dot{q}_i) d\sigma + K_{di}(\dot{q}_{id} - \dot{q}_i). \tag{5}$$

The desired velocity signals $\dot{q}_{id}$ are decoded from the received wave variables υ_m and u_s as

$$\dot{q}_{md} = \frac{1}{b}\tau_{mc} - \sqrt{2b}\upsilon_m, \quad \dot{q}_{sd} = \sqrt{2b}u_s - \frac{1}{b}\tau_{sc} \tag{6}$$

where $b > 0$ is the characteristic wave impedance that can be tuned to trade off the speed of motion with levels of force [12]. The received wave variables υ_m and u_s are related to the transmitted wave variables by

$$\begin{aligned} u_m &= \sqrt{2b}\tau_{mc} - \upsilon_m, \quad \upsilon_s = \sqrt{2b}\tau_{sc} - u_s \\ u_s &= u_m^{T_m}, \quad \upsilon_m = \upsilon_s^{T_s}. \end{aligned} \tag{7}$$

Wave reflections are eliminated by selecting $b = K_{di}$, appearing in (5), such that (6) reduces to

$$\dot{q}_{id} = \frac{1}{2}\left(\dot{q}_j^{T_j} + \dot{q}_i\right). \tag{8}$$

Hence, the reference velocity $\dot{q}_{id}$ used in the controller (5) is not equal to $\dot{q}_j(t - T_j)$, but half of the desired velocity $\dot{q}_{id}$ depends on the current velocity of the same device. This affects motion tracking performance, as our results in Section V indicate. Moreover, this controller lacks asymptotic position tracking due to the absence of position information in the wave variables [12].

C. Wave Variables + Position Tracking architecture (WT)

Position tracking in the wave variable architecture can be realized by using proportional terms outside the wave domain, as presented in, e.g., [2], [27], and [28]. In contrast to the original wave variables scheme, but similar to the PDd controller, local damping injection is then required to guarantee stability in the presence of delays, and consequently, delay-induced forces occur. The WT controller is given by

$$\tau_{ic} = K_{pi}\left(q_j^{T_j} - q_i\right) + K_{di}(\dot{q}_{id} - \dot{q}_i) - B_i\dot{q}_i. \tag{9}$$

Following the analysis in [2], stability is guaranteed if the controller parameters satisfy the inequality:

$$2B_m B_s > K_{pm}K_{ps}\left(T_m^2 + T_s^2\right). \tag{10}$$

D. Position–Force architecture (P-F)

In the P-F architecture (see [8], [9]), the slave synchronizes its motion with that of the master, whereas the master controller directly reflects the measured slave-environment interaction force, i.e.,

$$\tau_{mc} = -\tau_e^{T_s} - B_m\dot{q}_m \tag{11a}$$

$$\tau_{sc} = K_{ps}\left(q_m^{T_m} - q_s\right) + K_{ds}\left(\dot{q}_m^{T_m} - \dot{q}_s\right) - B_s\dot{q}_s. \tag{11b}$$

The local damping term B_i is included to aim at stable slave-environment interaction and to attenuate a recoiling of the master after the slave-environment impact.

E. Position/Force-Force architecture (PF-F)

The Position/Force-Force architecture is an extension of the P-F architecture and is given by (see [29])

$$\tau_{mc} = -\tau_e^{T_s} - B_m\dot{q}_m \tag{12a}$$

$$\tau_{sc} = \tau_h^{T_m} + K_{ps}\left(q_m^{T_m} - q_s\right) + K_{ds}\left(\dot{q}_m^{T_m} - \dot{q}_s\right) - B_s\dot{q}_s. \tag{12b}$$

Compared to the P-F controller (11), the operator force τ_h is used here in the slave-side controller. The use of τ_h improves motion tracking performance and the accuracy of the reflected contact stiffness (see [29] and our results in Section V). Similar to the P-F controller, the local damping term B_i is employed to realize stable slave-environment interaction.

F. Four-Channel architecture (4C)

As analyzed in [8], the four-channel controller provides optimal tracking and force reflection properties in the delay-free case. The controller is given by

$$\tau_{mc} = -\tau_e^{T_m} + K_{pm}\left(q_s^{T_s} - q_m\right) + K_{dm}\left(\dot{q}_s^{T_s} - \dot{q}_m\right) - B_m\dot{q}_m \tag{13a}$$

$$\tau_{sc} = \tau_h^{T_m} + K_{ps}\left(q_m^{T_m} - q_s\right) + K_{ds}\left(\dot{q}_m^{T_m} - \dot{q}_s\right) - B_s\dot{q}_s. \tag{13b}$$

When subject to delays, however, the four-channel controller suffers from delay-induced forces, caused by the motion synchronization term in τ_{mc}.

Remark 2: To the best of the authors' knowledge, no analytic stability results exist for the controllers presented in Sections III-D–III-F. Therefore, in order to realize a stable teleoperator during free motion, contact, and impact (i.e., the transition between free motion and contact) phases, a careful controller tuning is required, see Section IV-C below.

IV. Experimental Design and Evaluation

The six control architectures, presented in Section III, are compared experimentally for six different values of the communication delay. The delays are selected as $T_m = T_s \in \{0, 5, 10, 20, 35, 50\}$ ms, such that a trend in performance decrease per controller can be distinguished.

Authorized licensed use limited to: ASML Netherlands B.V.. Downloaded on August 07,2020 at 07:40:17 UTC from IEEE Xplore. Restrictions apply.

The main goal of this comparison is to highlight the key differences in performance between controllers, as a function of the communication delay, for specific bilateral teleoperation tasks. To this end, two sets of experiments are conducted to analyze the performance: one for the free motion phase and the other for the contact phase.

The evaluation of the performance of a specific controller-task-delay combination depends on the manipulation capabilities of the human operator. For a fair comparison of the *controller performance*, independent of the human operator, it is desired that each of the 36 combinations (six controllers times six delay values) is performed with an identical operator input. To cancel out as many variations in the results as possible due to, e.g., learning effects, operator fatigue, or variability between trials and operators, it is decided not to perform the comparison with actual human operators. Instead, a *virtual operator*, presented in (14), is used to achieve the desired fairness in performing the experiments repeatedly.

A. Experimental Design

Free Motion: For the free motion experiments, we use a virtual operator to prevent variations in the results caused by different human operators. The operator model comes from an extensive identification study in [23, Sec. 2.1], where the interaction of several human operators with the same master device as we used in this paper has been analyzed. The resulting operator model is, therefore, tailored to the considered experimental setup and is given by

$$\tau_h = L(k_h(q_d - q_m) + b_h(\dot{q}_d - \dot{q}_m)) + m_h\ddot{q}_d \qquad (14)$$

where $k_h = 8$ Nm/rad and $b_h = 0.1$ Nms/rad correspond to a slightly firm grasp. The virtual operator performs a positioning task by moving the master device according to a desired profile q_d. The desired motion profile q_d is designed to encompass a realistic range of frequencies of human input and consists of a sine-sweep from 0.1 to 1 Hz [30]. The desired trajectory is shown in Fig. 3. The feedforward term $m_h\ddot{q}_d$ in (14) represents the operator's internal model of the system and is selected as $m_h = 18.2 \cdot 10^{-3}$ kg/m^2, close to the identified inertia in [23]. Finally, the low-pass filter L, having a cutoff frequency of 10 Hz, represents the operator's limited capabilities to apply a high-frequency force profile, despite his intention and sensing capabilities. By using such an operator model, we obtain the required fairness in the results in Section V. Due to the fact that the model in (14) comes from identification experiments, we accurately include the main dynamical operator characteristics during free motion.

Contact: In the contact experiments, the slave is initially positioned against an aluminum cylinder, as shown in Fig. 2, and does not break contact during the experiment. To achieve a realistic, yet consistent experiment, an operator torque profile is recorded from the setup by manually providing force to the end-effector of the master device, while the slave is in contact with the environment. This recorded torque signal, shown in Fig. 4, ranges from 0 to about 0.7 Nm and is used in all 36 experiments as the torque applied by the virtual operator. The original measurement noise is filtered from this profile by means of an off-line zero-phase-lag filtering technique.

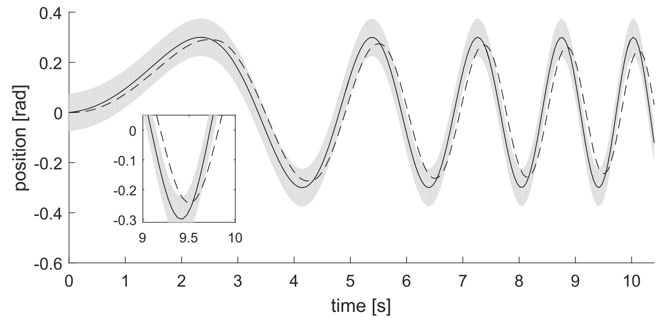

Fig. 3. Free motion desired operator trajectory q_d (solid line), the allowable region (gray area), and an example of the master position q_m (dashed line) from an experiment with a PDd controller and $T_j = 10$ ms delay. Due to delay-induced forces, q_m lags q_d, clearly visible in the zoomed-in box.

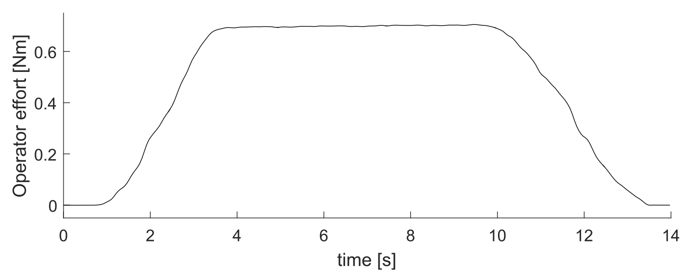

Fig. 4. Applied operator torque τ_h during the contact experiments.

Remark 3: Variations in k_h in (14) (which is the most sensitive parameter between operators [23]) does not affect stability in free motion for all architectures except 4C. In particular, the stability results for the PDd, W, and WT architectures are independent of the operator (which is assumed to be passive). The P-F and PF-F architectures are unilateral in free motion and hence stable, even without injected damping, for any operator. For the impact and contact phases, a lower value for k_h (i.e., a looser grip of the operator) may require slightly larger damping gains to warrant stability (the same holds for the 4C architecture in free motion due to the lack of analytical stability results), so careful tuning in practice is important. However, the relative difference and performance degradation of the controllers as a function of the delay, presented in Section V, are expected to be similar to the results presented here.

B. Performance Metrics

Several ways of capturing teleoperator performance have been presented in the literature, e.g., transparency (the degree to which the operator can feel through the teleoperator as if she/he is interacting with the environment directly), see [8], or Z-width (the range of impedances that can be reflected to the operator), see [31]. The measurable performance metrics used in this paper are based on the ones used in [17], [18], and [20] to separately evaluate performance in the free motion and contact phases. In addition, a new metric to describe the operator effort in free motion is introduced below.

Authorized licensed use limited to: ASML Netherlands B.V.. Downloaded on August 07,2020 at 07:40:17 UTC from IEEE Xplore. Restrictions apply.

Free Motion: In free motion, the main goal of the controller is to make the slave track the motion of the master. In order to capture the motion tracking performance in a single metric, the root mean square (RMS) of the position tracking error between master and slave, $q_m - q_s$, is employed, i.e.,

$$\Delta q_{rms} := \sqrt{\frac{T_s}{\Delta t}\sum_{t=t_0}^{t_f}(|q_m(t) - q_s(t)|^2)} \tag{15}$$

with $\Delta t = t_f - t_0$, t_0 is the start of the experiment, t_f is the end of the experiment, and $T_s = 5 \cdot 10^{-4}$ s is the sampling time. Due to a discrete implementation, the sum of the tracking error at each time instant t is used in the metric.

In the presence of delays, the position of the master q_m is transmitted to the slave controller at time t, but arrives T_m seconds later. Because q_m is not directly available on the slave side, a second motion tracking metric is defined that is related to the motion tracking error $q_m^{T_m} - q_s$ of the slave controller, i.e.,

$$\Delta q_{rms}^{T_m} := \sqrt{\frac{T_s}{\Delta t}\sum_{t=t_0}^{t_f}(|q_m(t - T_m) - q_s(t)|^2)}. \tag{16}$$

This metric provides different results than (15), as our comparison in Section V illustrates, and to the best of the authors' knowledge, this metric has not been used in previously reported comparison studies.

For the free motion experiments, we introduce a new metric, namely the effort provided by the operator to manipulate the teleoperator. A high operator effort is related to a higher level of fatigue and should be avoided in practice. For the free motion experiments, the operator effort is described by the RMS value of the torque τ_h applied by the operator on the master device, i.e.,

$$\tau_{h,rms} := \sqrt{\frac{T_s}{\Delta t}\sum_{t=t_0}^{t_f}(|\tau_h(t)|^2)}. \tag{17}$$

To the best of the authors' knowledge, such a metric has not been used in previous comparison studies.

Contact: When the slave is in steady contact with a stiff environment, it is a key that the operator force τ_h is applied on the environment and that the slave-environment interaction force τ_e is accurately reflected to the operator. Therefore, the RMS of the force tracking error $\tau_h - \tau_e$ is evaluated. The contact task consists of parts where the torque applied by the virtual operator increases or decreases (dynamic part) and a part where it is kept constant (static part). Consequently, two metrics are used, i.e.,

$$\Delta \tau_{rms} := \sqrt{\frac{T_s}{\Delta t}\sum_{t=t_0}^{t_f}(|\tau_h(t) - \tau_e(t)|^2)} \tag{18a}$$

$$\Delta \tau_{rms,ss} := \sqrt{\frac{T_s}{\Delta t_{ss}}\sum_{t=t_{0,ss}}^{t_{f,ss}}(|\tau_h(t) - \tau_e(t)|^2)} \tag{18b}$$

where $t_{0,ss} = 3.7$ s and $t_{f,ss} = 9.5$ s represent the start and end of the steady-state window of the static interval, respectively, and $\Delta t_{ss} = t_{f,ss} - t_{0,ss}$. Hence, metric (18a) evaluates the performance over the whole contact experiment, whereas metric (18b) describes the performance during the static phase only. Unlike metrics (15) and (16), no difference was observed when using either the undelayed (τ_h) or the delayed ($\tau_h^{T_m}$) torque signals in (18). Therefore, only metrics with τ_h are considered here.

Apart from synchronizing τ_h and τ_e, the controller should also properly reflect the stiffness of the environment to the operator. For contact with a rigid environment, the stiffness reflected to the operator is similar to the stiffness of the teleoperator (caused by the device drive trains and the controller itself, the latter dominating the results in this comparison). The performance metric of the teleoperator stiffness is the RMS value of the ratio of the applied operator force τ_h, and the position difference between the master and the slave. Similar to the force reflection metrics (18), performance is analyzed for both the whole experiment and the static part only:

$$S_{rms} := \sqrt{\frac{T_s}{\Delta t}\sum_{t=t_0}^{t_f}\left(\left|\frac{\tau_h(t)}{q_m(t) - q_s(t)}\right|^2\right)} \tag{19a}$$

$$S_{rms,ss} := \sqrt{\frac{T_s}{\Delta t_{ss}}\sum_{t=t_{0,ss}}^{t_{f,ss}}\left(\left|\frac{\tau_h(t)}{q_m(t) - q_s(t)}\right|^2\right)}. \tag{19b}$$

Remark 4: Although the end-effector position of the slave remained constant during the experiments, a position difference of $14 \cdot 10^{-4}$ rad is measured by the encoder on the motor shaft due to the finite stiffness of the drive train of the slave. However, this barely influences the results since the controller stiffness is much lower than the stiffness of the teleoperator.

C. Tuning

First and foremost, a teleoperator must be stable during the free motion, contact, and impact phases. Moreover, the force applied by a human operator in free motion cannot be too high (such that comfortable operation becomes impossible), and the operator must be able to keep the slave in contact with the environment. Due to the delay-induced forces and the associated operator effort, the free motion phase is the most critical with respect to controller tuning for the PDd, WT, and 4C architectures. The contact phase (in particular, the impact and detachment phases) is the most critical to the P-F and PF-F controllers due to the recoiling.

A strict procedure is maintained to tune the controller parameters of each architecture-delay combination. In this procedure, performance is reduced, if necessary, to achieve stability during the free motion, impact, and contact phases. In free motion, a similar master motion is pursued for all controller-delay combinations, see Fig. 3. That is, we require that the master position q_m stays within 30% (0.09 rad) of the amplitude of the desired trajectory q_d at all times, indicated by the gray area in Fig. 3. For the PDd, WT, and 4C architectures, the delay-induced forces are the most critical to satisfy this requirement. As discussed in Remark 1, the delay-induced forces increase with a larger value of K_{pm} and a larger value of the delay. For increasing values of the delay, the delay-induced

Authorized licensed use limited to: ASML Netherlands B.V.. Downloaded on August 07,2020 at 07:40:17 UTC from IEEE Xplore. Restrictions apply.

TABLE I
CONTROL PARAMETERS USED FOR THE EXPERIMENTS

Contr.	Param.	0ms	5ms	10ms	20ms	35ms	50ms
PDd	K_{pi}	17	17	13	7	4	3
	K_{di}	0.1	0.1	0.1	0.1	0.1	0.1
	B_i	0	0.032	0.055	0.061	0.061	0.068
W	K_{pi}	17	17	17	17	17	17
	$K_{di} = b$	0.1	0.1	0.1	0.1	0.1	0.1
WT	K_{pi}	17	15	11	5.5	3	2.5
	$K_{di} = b$	0.1	0.1	0.1	0.1	0.1	0.1
	B_i	0	0.053	0.065	0.07	0.072	0.078
P-F & PF-F	K_{ps}	8	8	8	8	8	8
	K_{ds}	0.1	0.1	0.1	0.1	0.1	0.1
	B_m	0	0.01	0.03	0.08	0.18	0.25
	B_s	0	0.01	0.01	0.02	0.06	0.1
4C	K_{pi}	17	17	17	17	11	8
	K_{di}	0.1	0.1	0.1	0.1	0.1	0.1
	B_m	0	0.01	0.01	0.01	0.01	0.01
	B_s	0.02	0.02	0.04	0.04	0.04	0.04

force becomes too large, and the (virtual) operator is not able to track the reference q_d within the specified bounds. In order to achieve the desired tracking accuracy (as in Fig. 3) again, the delay-induced forces need to be reduced by lowering K_{pm} sufficiently. An example of a master position q_m that does not track the desired motion q_d within the specified bounds, due to too high delay-induced forces (and thus requires a reduction of K_{pi}), is shown in Fig. 3, with a dashed line.

We emphasize that all controllers are tuned such that, *when operated by a real human operator*, the free motion, contact, and *impact* (i.e., the transition from free motion to contact) phases are stable, and a recoiling of the master, due to the impact or detachment of the slave with the environment, does not occur. A real human operator has been chosen for this part of the tuning procedure due to the lack of analytic stability results for the P-F, PF-F, and 4C architectures under the influence of delays. In this way, realistic damping gains are obtained that effectively stabilize the impact and contact phases for these architectures. We emphasize that the actual fee motion experiments used for the performance comparison analysis are all performed with the virtual operator (14).

Consider Table I. In the tuning procedure, all architectures start with the same nominal parameter values for the delay-free case (see the third column of Table I), namely $K_{pi} = 17$ Nm/rad, $K_{di} = 0.1$ Nms/rad, and $B_i = 0$ Nms/rad. For the W and WT architectures, the wave impedance is set to $b = K_{di} = 0.1$ Nms/rad to eliminate wave reflections. Then, for increasing values of the delay, the parameters K_{pi} and B_i are adjusted to prevent instability, a recoiling of the master, or violating sufficient tracking of the desired reference q_d by the master device in free motion (due to the delay-induced forces and the associated large operator effort). For each controller-delay combination, we choose $K_{pm} = K_{ps}$ to prevent motion or force scaling.

We will now discuss the tuning procedure for the different control architectures. The architectures PDd, WT, and 4C suffer from delay-induced forces in free motion due to a motion tracking term in the master controller. For increasing values of the delay, these architectures are tuned to limit the operator effort in order to satisfy the tracking requirement of q_d by the master device sufficiently, see Fig. 3. If necessary, the proportional gains K_{pi} are lowered, compared with the previous (lower) delay value, such that q_m resides within the 30% accuracy bound on q_d. The local damping gain is then selected to just satisfy (3) and (10) for the PDd and WT controllers, respectively. For the 4C controller, the damping gains are tuned manually to obtain stability during all phases due to the lack of an analytic stability bound.

To the best of the authors' knowledge, no analytic stability criteria exist for the direct force-reflecting architectures P-F and PF-F. We aim at finding a fair tradeoff between the proportional and damping gains, in order to stabilize the system on one hand, and achieve satisfactory performance on the other hand. In particular, recoiling of the master device is more severe for higher proportional gains. In order to achieve stable contact, high damping gains are then required, which, in turn, negatively influence tracking performance and operator effort in free motion. In order to limit the damping gains (and the resulting operator effort) while still achieving satisfactory performance with the P-F and PF-F architectures, we select $K_{pi} = 8$ Nm/rad. Then, for each delay value, the damping gains B_i are tuned to prevent a recoiling when the teleoperator is operated by a real human.

The parameter values obtained from this tuning procedure for each controller-delay combination are presented in Table I. For each combination, the same values are used in both the free motion and contact experiments.

Remark 5: The tuning of the controller parameters has a significant influence on the performance that can be achieved. Recall that, in this paper, it is by no means attempted to obtain optimal tuning for each presented controller-delay combination. Instead, the tuning illustrates the basic level of performance that can be achieved and highlights the differences between the considered architectures. The authors are aware that with optimal tuning, one controller might perform better than another, but this will not affect the conclusions drawn in Section V. A different nominal tuning (i.e., control parameters at zero delay) does not alter the relative difference in performance along with controllers due to the strict tuning procedure described above.

V. EXPERIMENTAL RESULTS

The results of the free motion and contact experiments are presented in this section. First, some time plots are discussed to illustrate the differences in behavior when using the controllers introduced in Section III. Subsequently, the performance metrics of Section IV-B are evaluated.

A. Time Plots

Free Motion: In order to illustrate the differences in behavior of the controllers, the desired motion q_d, master position q_m, slave position q_s, and operator torque τ_h of the free motion experiments are shown in Fig. 5 for the PDd, W, PF-F,

Authorized licensed use limited to: ASML Netherlands B.V.. Downloaded on August 07,2020 at 07:40:17 UTC from IEEE Xplore. Restrictions apply.

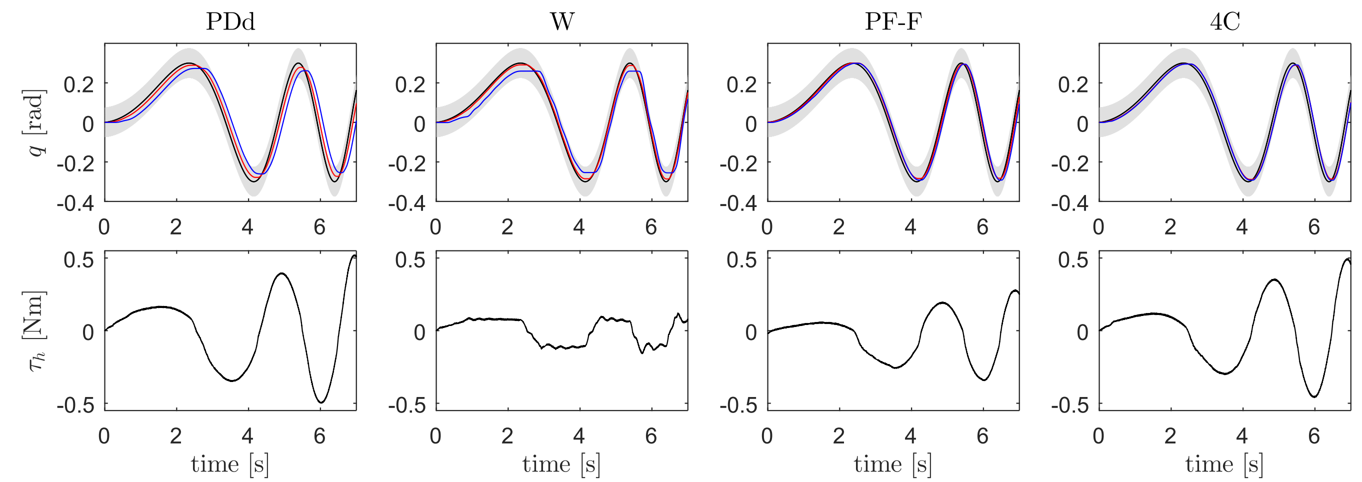

Fig. 5. Free motion experiments: position and operator effort profiles of the selected controllers ($T_m = T_s = 50$ ms). The black, red, and blue lines indicate q_d, q_m, and q_s, respectively. The gray area is the allowable region for q_m. Only the first 7 s of the experiments are plotted to improve visibility.

and 4C architectures, and a one-way communication delay of $T_m = T_s = 50$ ms.

For the PDd architecture, there is a visible lag between q_m (red line) and q_d (black line), as well as between q_s (blue line) and q_m. This lag is mainly caused by the relatively small proportional gains K_{pi} (see Table I), selected to limit the delay-induced forces resulting from the master side PD-controller, to keep the operator effort bounded. Even so, τ_h is relatively large compared with the PF-F controller and q_m and q_s do not track the amplitudes of q_d around direction changes. The response of the WT-controlled teleoperator is similar to the PDd results since the derivative action is small compared with the proportional action and is, therefore, not reported.

The W-controlled teleoperator requires the least operating effort (smallest τ_h) due to the absence of delay-induced forces because no damping is injected by the controller. The slave position q_s differs from the master position q_m, especially around position reversals, because only velocity signals are used in the wave variables, and consequently, the controller lacks asymptotic position tracking capabilities. For low velocities, the computed torques τ_{mc} and τ_{sc} are not large enough to overcome the static friction of the devices.

The operator effort for the P-F and PF-F controllers is identical since, in both cases, τ_h is only affected by the injected damping. Due to the use of τ_h in τ_{sc} of the PF-F controller (12), the slave follows the master motion accurately, apart from the 50-ms delay. The motion tracking with the P-F architecture is not as good as with the PF-F scheme, illustrating the advantage of using τ_h in the slave-side controller.

The 4C architecture realizes a small tracking error $q_m - q_s$ due to the use of τ_h in τ_{sc} in (13). Moreover, q_s tracks the amplitude of q_d accurately, despite the relatively high operating effort caused by the delay-induced forces. The operator effort τ_h looks similar to those of the PDd and WT controllers because, for the latter two architectures, the controller gains are lower, compared with the 4C controller, in order for the master to track q_d within the specified bounds.

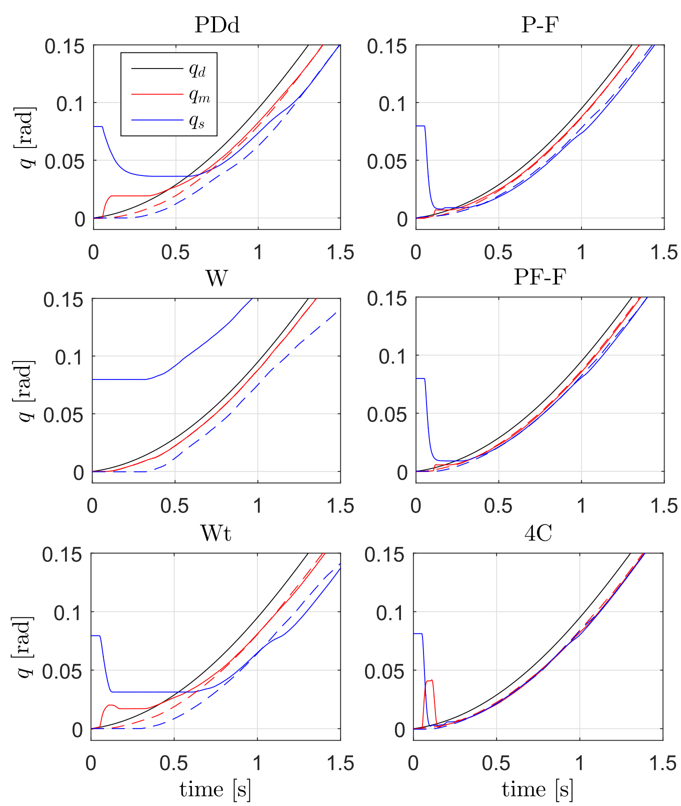

Fig. 6. Position profiles of two free motion experiments ($T_m = T_s = 50$ ms) with different initial positions for the slave.

For $T_m = T_s = 50$ ms, Fig. 6 shows the effect on the motion tracking and convergence of an initial offset in the master and slave positions. The dashed lines are obtained from experiments where the initial master and slave positions are identical, whereas for the solid lines, the slave started with an offset of 0.08 rad compared to the master. In both experiments, the same desired operator signal q_d is used. For the experiments with an initial position offset, the master position is initialized for the interval $\theta_i := [-T_i, 0)$ at $q_m(\theta_m) = 0$

Authorized licensed use limited to: ASML Netherlands B.V.. Downloaded on August 07,2020 at 07:40:17 UTC from IEEE Xplore. Restrictions apply.

rad, and the slave position is initialized at $q_s(\theta_s) = 0.08$ rad. At time $t = 0$ s, the actual master and slave positions are transmitted. These signals arrive 50 ms later at the other side.

For all architectures, except the W-controller (which lacks asymptotic position tracking capabilities), the master and slave positions converge to the same trajectories, independent of the initial positions. The convergence time differs per architecture and is related inversely proportionally to K_{pi}.

For the PDd and WT architectures, K_{pi} is relatively low, such that the convergence is relatively slow. Furthermore, the architectures PDd, WT, and 4C have motion feedback terms in both controllers. As a result, *both* the master and the slave start to move to the *delayed* position of the other device after $t = 0.05$ s. Because the master device moves away from q_d, the virtual operator reacts and increases τ_h to move q_m back to q_d. In the 4C controller, this increased τ_h is transmitted to the slave and results in a larger initial slave movement compared with the PDd and WT controllers. The master controllers of the P-F and PF-F controllers do not contain motion tracking terms. Therefore, the master position is barely affected by the initial position offset, and the slave converges to the master position.

Contact: For the contact experiments, the master and slave position and torque signals are visualized in Fig. 7 for $T_m = T_s = 50$ ms. In theory, all architectures should be able to accurately reflect the slave-environment interaction torque to the operator (i.e., $\tau_h = \tau_e$) during the static phase. The observed deviation from $\tau_h = \tau_e$ during the static phase and at the end of the experiment is of the same order for all architectures and is mainly caused by static friction in the drive train. Therefore, the main focus in the analysis is on the dynamic torque tracking and stiffness reflection.

The PDd architecture has a lag larger than 50 ms between τ_e and τ_h. This is mainly caused by the low K_{pi} value and, to a lesser extent, by the injected damping. Since no torque information is present in (2), the controllers at both sides require a difference in master and slave positions to generate the requested torques. The maximum position difference of 0.225 rad for $\tau_h = 0.695$ Nm results in a perceived stiffness of 3.1 Nm/rad for the PDd architecture. For the WT architecture, the reflected stiffness is 2.8 Nm/rad. In comparison, the reflected stiffness in the delay-free case is 17 and 20 Nm/rad for the PDd and WT architectures, respectively. As expected, the reflected stiffness is close to the values of K_{pi}.

Although the W architecture has comparable torque tracking performance to the PDd and WT controllers, the difference in stiffness reflection is large. Since the W architecture lacks asymptotic position synchronization, and due to the difference between $\dot{q}_j^{T_j}$ and $\dot{q}_i$ in (8), the reflected stiffness is 1.55 Nm/rad at 50 ms delay, despite the relatively high values of K_{pi}. For the delay-free case, the reflected stiffness is 8 Nm/rad.

The reflected stiffness of the P-F architecture is 8.2 Nm/rad. This reflected stiffness is independent of the delay since $K_{ps} =$ 8 Nm/rad for all delay cases. A remarkable result is formed by the "stairs" in τ_e and q_m during dynamic torque tracking. This effect is not present in the delay-free case but increases in size for increasing delay values. The effect is related to the start of a recoiling of the master due to a build-up of the slave-environment interaction force and the delay in the force reflection to the operator. The static friction in the slave amplifies the sensitivity to the recoiling, but a full recoiling is prevented by the injected damping.

For both the PF-F and 4C controllers, the torque tracking and reflected stiffness are comparable. Due to the transmission of both τ_h and τ_e (which are the dominant signals for stiffness reflection), these architectures have, by far, the best stiffness reflection and torque tracking during the dynamic part of the experiments. During the static phase, a reflected stiffness of about 700 Nm/rad was achieved for both architectures.

B. Performance in Free Motion

1) Motion Tracking: Fig. 8(a) shows the motion tracking performance, for each controller-delay combination, according to Δq_{rms} and $\Delta q_{rms}^{T_m}$, defined in (15) and (16), respectively. A decrease of the proportional gains K_{pi} *with respect to the previous delay value* is indicated by a dashed line between two subsequent points, whereas a solid line indicates unaltered gains. The blue lines represent the bilateral motion synchronization architectures (which do not use force sensor information). The red lines represent the direct force-reflection schemes and the bilateral motion synchronizing 4C architecture, all using force sensor information.

Both plots show that motion tracking performance decreases (i.e., a larger value for Δq_{rms} and $\Delta q_{rms}^{T_m}$) for increasing delays. This decrease is not only caused by the delay in receiving the position, torque, or wave variables from the other side. For the PDd, WT, and, to a lesser extent, 4C architectures, the performance is also affected by the reduction of K_{pi} to prevent high operator efforts, in order for the master to track q_d within the specified bounds. For the W architecture, the performance decrease is partly affected by the increasing difference of $\dot{q}_j^{T_j}$ and $\dot{q}_i$ in (8) for increasing delays. For the P-F and PF-F controllers, the motion tracking performance is affected by the increase in injected damping for increasing delays.

When comparing the results of Δq_{rms} with $\Delta q_{rms}^{T_m}$, it is observed that the differences in performance of all controllers are smaller for the latter metric. The PDd and WT controllers score better for $\Delta q_{rms}^{T_m}$ due to the low values of K_{pi}. These values are typically so low (to bound the operator effort) that the lag in tracking q_m by the slave is larger than T_m. The P-F and PF-F schemes perform best on $\Delta q_{rms}^{T_m}$ since these architectures are designed to control the error $q_m^{T_m} - q_s$ to zero instead of the error $q_m - q_s$, as is the case for the PDd, WT, and 4C architectures. A remarkable result is the significant difference between the metrics $\Delta q_{rms}^{T_m}$ and Δq_{rms} for the 4C architecture. This clearly shows that adding a motion synchronizing term to the master controller changes the control goal with respect to the PF-F controller, i.e., the motion tracking error that is controlled.

2) Operator Effort: The RMS values of the operator effort, $\tau_{h,rms}$, as a function of the delay, are presented in Fig. 8(b). Apart from the W architecture, the operator effort increases

Authorized licensed use limited to: ASML Netherlands B.V.. Downloaded on August 07,2020 at 07:40:17 UTC from IEEE Xplore. Restrictions apply.

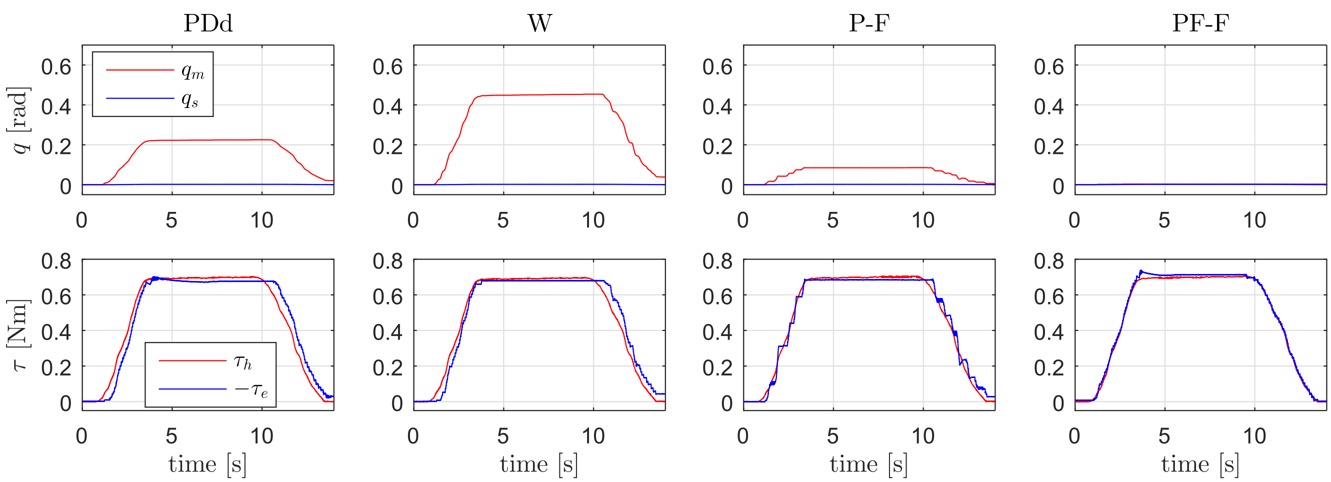

Fig. 7. Contact experiments: position (top) and torque (bottom) profiles of the PDd, W, P-F, and PF-F architectures ($T_m = T_s = 50$ ms). The response of the WT and 4C architectures is similar to the response of the PDd and PF-F controllers, respectively, and is, therefore, omitted.

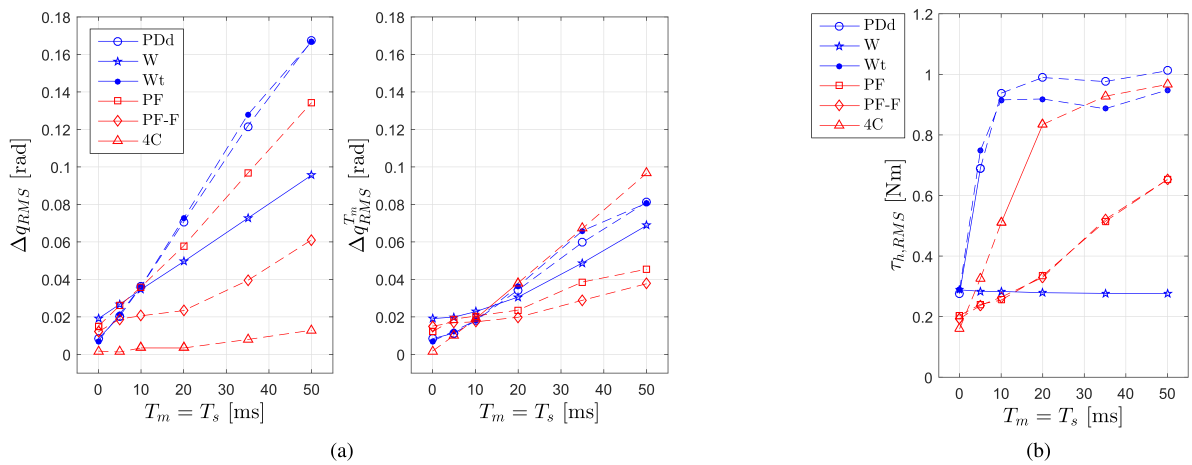

Fig. 8. Performance metrics as a function of the communication delay for the free motion experiments. (a) RMS values of the free motion tracking errors as a function of the communication delay are presented. The left subplot shows Δq_{rms}, defined in (15), whereas the right subplot shows $\Delta q^{T_m}_{\text{rms}}$, defined in (16). (b) RMS values of the free motion operator effort $\tau_{\text{h,rms}}$, defined in (17), are presented.

(higher $\tau_{h,rms}$) for increasing values of the delay. For the P-F and PF-F architectures, the increase in operator effort is solely caused by the injected damping necessary to ensure stability in the contact phase. For the PDd, WT, and 4C architectures, the increase in operator effort is mainly due to the delay-induced forces. The saturation is the result of the tuning procedure: the values of the proportional controller gains are reduced to limit the operator effort, such that the master position does not exceed the specified bound on q_d. Reducing K_{pi}, however, negatively influences the motion tracking performance [see Fig. 8(a)].

Compared to PDd and WT, the additional use of τ_h in τ_{sc} by the 4C controller (13) results in a reduced motion tracking error. In turn, as a result of lower delay-induced forces, a reduction in operator effort is obtained. Note that the difference in the damping gains B_i between the controllers has a smaller effect on the operator effort than the delay-induced forces.

The operator effort for the W architecture is unaffected by the delay due to the absence of delay-induced forces. Hence, the controller gains are kept constant throughout the W experiments.

C. Performance in Contact

1) Torque Tracking: The RMS values of the torque tracking error are shown in Fig. 9(a) for both the full experiments, $\Delta\tau_{rms}$, and for the static part considered separately, $\Delta\tau_{rms,ss}$. Due to the static friction in the drive train, there are relatively large differences in $\Delta\tau_{rms,ss}$ per controller for different delay values [see the right plot in Fig. 9(a)]. As a result, no significant differences are observed in the steady-state torque tracking. When looking at the full experiments in the left plot of Fig. 9(a), it can be seen that, even though the torque signals are not perfect (e.g., due to measurement noise and calibration offsets), the architectures that use force sensor information have better dynamic torque tracking, compared to the architectures that do not use force sensor information.

For the PDd and WT architectures, the dynamic torque tracking is poor for $T_i > 5$ ms, due to the relatively low value

Authorized licensed use limited to: ASML Netherlands B.V.. Downloaded on August 07,2020 at 07:40:17 UTC from IEEE Xplore. Restrictions apply.

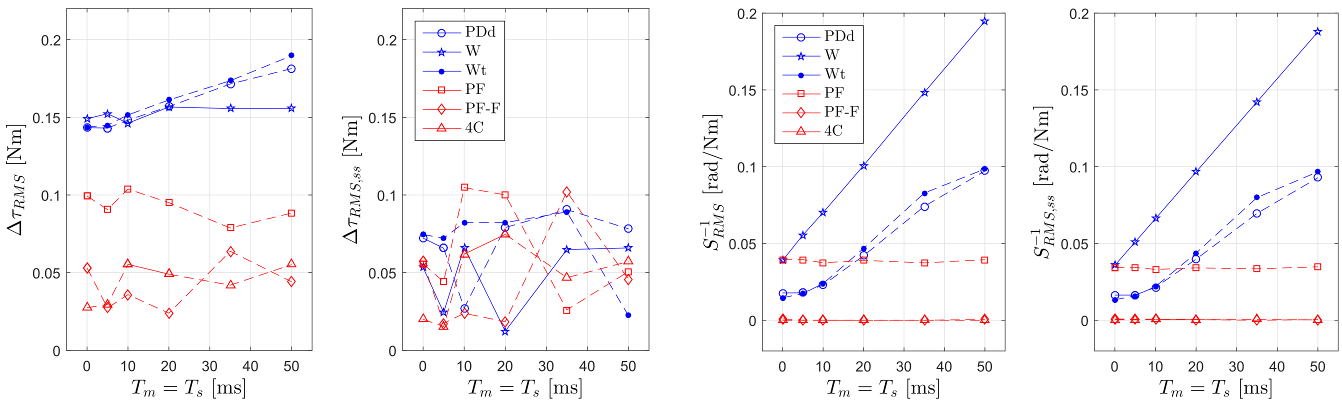

(a) (b)

Fig. 9. Performance metrics as a function of the communication delay for the contact experiments. (a) RMS values of the torque tracking errors in contact. The left subplot shows the torque tracking performance $\Delta\tau_{\text{rms}}$ defined in (18a), and the right subplot illustrates the static torque tracking performance $\Delta\tau_{\text{rms,ss}}$ defined in (18b). (b): RMS values of the reflected stiffness in contact. The left subplot shows S^{-1}_{rms}, the inverse of the reflected stiffness during the whole contact experiment, defined in (19a). The right subplot shows $S^{-1}_{\text{rms,ss}}$, the inverse of the reflected stiffness during the static part, defined in (19b).

for K_{pi}. The value of $\Delta\tau_{rms}$ increases proportionally with the delay, due to the applied tuning to bound the operator effort in free motion. For the W architecture, $\Delta\tau_{rms}$ depends less on the delay, and the torque tracking is better for higher delay values, compared to the PDd and WT architectures. The large difference between $\Delta\tau_{rms}$ and $\Delta\tau_{rms,ss}$ for the PDd, W, and WT architectures is the result of the relatively poor torque tracking during the dynamic parts.

Despite the "stairs" in τ_e and q_m (see Fig. 7), the dynamic torque tracking performance of the P-F controller is better than for the PDd, W, and WT architectures. Since K_{ps} is kept constant for all delay values, the dynamic torque tracking is independent of the delay value (the variation for different delays occurs in the static phase). Finally, the PF-F and 4C controllers yield the best overall torque tracking due to the use of τ_e in the master controller, and τ_h in the slave controller.

2) Stiffness Reflection: In Fig. 9(b), the inverse of the reflected stiffness S_{rms} and $S_{rms,ss}$, defined in (19a) and (19b), respectively, are presented. The inverse of this metric is used so that, similar to the previous results, a lower value indicates a better performance. It is observed that for all architectures the performance of the reflected environment stiffness is similar to both the static part (right subplot) and the dynamic part (left subplot).

For the PDd, W, and WT architectures, the ability to reflect the environment stiffness to the operator degrades with an increasing delay. For the PDd, WT, and P-F controllers, the performance is proportionally related to K_{pi}, i.e., a higher value results in a better stiffness reflection. The stiffness reflection is affected for the PDd and WT controllers due to the reduction of K_{pi}, required to limit the delay-induced forces in the free motion phase. The reflected stiffness of the W architecture is affected by the lack of position tracking terms in the controller. Due to the increasing difference of $\dot{q}_j^{T_j}$ and $\dot{q}_i$ in (8), the motion error $q_m - q_s$ increases proportionally with the delay, such that the reflected stiffness is poor when the delay increases. This illustrates the importance of position tracking in bilateral motion synchronization architectures when stiffness reflection is required.

For the current experiments and tuning, the PF-F and 4C controllers provide the best stiffness reflection. Moreover, the performance of these architectures in terms of stiffness reflection seems to be insensitive to delays. Due to the use of τ_e and τ_h in the master and slave controllers, respectively, no position error between the master and the slave is required to generate the requested torques, so that the values of K_{pi} do not play a role for the perception of stiffness. Despite the drive train imperfections, limited encoder resolution, and measurement noise, the error $q_m - q_s$ never exceeded $1 \cdot 10^{-3}$ rad during the contact experiments.

Remark 6: For delays larger than 50 ms, the reported effects become even larger. For the current experimental setup, this may result in increased delay-induced, damping, or reflected environment forces, risking saturation of the control forces. However, a trend in the performance metrics for increasing delays is clearly visible in Figs. 8 and 9.

VI. Discussion

The experimental results show per metric a clear relation between the different controller classes and obtained performance for the considered one-DOF teleoperator. For the bilateral motion synchronization architectures, PDd, W, and WT, a performance loss due to time delays is present in *both* the free motion and contact phases. In contrast, the performance of the 4C, P-F, and PF-F controllers is only affected in free motion. The results indicate that the PF-F architecture gives the best overall performance in the sense that it is the least sensitive to delays. Note that this conclusion is independent of the controller tuning, as long as the teleoperator is stable.

In general, using the operator torque τ_h in the slave controller improves motion tracking. The P-F and PF-F architectures are designed specifically to control the error $q_m^{T_m} - q_s$ to zero. In contrast, all other controllers have motion synchronization terms in the master controller and instead seem to control the error $q_m - q_s$ to zero. Pursuing to control the

Authorized licensed use limited to: ASML Netherlands B.V.. Downloaded on August 07,2020 at 07:40:17 UTC from IEEE Xplore. Restrictions apply.

TABLE II

OVERVIEW OF THE PERFORMANCE PER METRIC, AT $T_m = T_s = 0$ s, RELATIVE TO THE ARCHITECTURE THAT PERFORMS WORST (INDICATED WITH 100%). THE 4C ARCHITECTURE PERFORMS BEST ON ALL METRICS. NOTE THAT $\Delta q_{rms}^{T_m} = \Delta q_{rms}$ SINCE $T_m = 0$ s

	Metric	PDd	W	Wt	P-F	PF-F	4C
free motion	Δq_{RMS}	44%	100%	37%	79%	63%	9%
	$\Delta q_{RMS}^{T_m}$	44%	100%	37%	79%	63%	9%
	τ_{RMS}	96%	100%	100%	71%	67%	55%
contact	$\Delta\tau_{RMS}$	96%	100%	96%	67%	36%	18%
	$\Delta\tau_{RMS,ss}$	-	-	-	-	-	-
	S_{RMS}^{-1}	45%	99%	37%	100%	2%	0%
	$S_{RMS,ss}^{-1}$	46%	100%	37%	96%	2%	1%

TABLE III

OVERVIEW OF THE PERFORMANCE DEGRADATION FOR INCREASING VALUES OF THE COMMUNICATION DELAY. THE PF-F ARCHITECTURE HAS THE SMALLEST PERFORMANCE DEGRADATION

	Metric	PDd	W	Wt	P-F	PF-F	4C
free motion	Δq_{RMS}	$\overline{\triangledown}$	$\overline{\triangledown}$	$\overline{\triangledown}$	$\overline{\triangledown}$	$\triangledown$	$\triangledown^*$
	$\Delta q_{RMS}^{T_m}$	$\overline{\triangledown}$	$\overline{\triangledown}$	$\overline{\triangledown}$	$\triangledown$	$\triangledown^*$	$\overline{\triangledown}$
	τ_{RMS}	$\overline{\triangledown}$	$\square^*$	$\overline{\triangledown}$	$\triangledown$	$\triangledown$	$\overline{\triangledown}$
contact	$\Delta\tau_{RMS}$	$\triangledown$	$\square$	$\triangledown$	$\square$	$\square^*$	$\square^*$
	$\Delta\tau_{RMS,ss}$	-	-	-	-	-	-
	S_{RMS}^{-1}	$\triangledown$	$\overline{\triangledown}$	$\triangledown$	$\square$	$\square^*$	$\square^*$
	$S_{RMS,ss}^{-1}$	$\triangledown$	$\overline{\triangledown}$	$\triangledown$	$\square$	$\square^*$	$\square^*$

$\square$: Performance not affected by delays.
$\triangledown$: Relatively small performance decrease for increasing delays.
$\overline{\triangledown}$: Relatively large performance decrease for increasing delays.
$*$: Best performance for this metric.

error $q_m - q_s$ to zero is accompanied by delay-induced forces. For both the PDd and WT controllers, limiting the operator effort in free motion by lowering K_{pi} results in a reduction of the reflected environment stiffness. For the 4C architecture, the reflected environment stiffness seems to be unaffected by the delay, but the controller suffers from delay-induced forces instead, resulting in a high operator effort for large delays. Therefore, from a performance point of view, the increased delay-induced forces make bilateral motion synchronization architectures less suitable for delayed bilateral teleoperation. Delay-induced forces are not present in the W controller, so that the operator effort is independent of the delay. Motion tracking performance and stiffness reflection are, however, significantly affected by the delays due to the absence of position tracking terms in the controller. Especially for reflecting the environment stiffness, these position tracking terms are key in bilateral motion synchronization architectures. The P-F and PF-F do not suffer from the delay-induced forces (due to the absence of a motion tracking term in the master controller), but require high damping gains to avoid a recoiling of the master during the free motion to contact transitions. Even with high damping gains for P-F and PF-F, the operator effort is lower for large delays compared with the 4C controller, showing the significance of delay-induced forces, compared to damping injection.

An overview of the relative performance without delays is presented in Table II. In the absence of delays, the 4C architecture performs best on all metrics, as already mentioned in [8]. An overview of the performance degradation per architecture as a result of delays is presented in Table III. For each metric, the performance is classified as a relatively large decay, a relatively small decay, or no decay for increasing delays. The distinction between a relatively small and large decay is determined by the mean of all nonzero decay rates. Overall, the PF-F architecture is affected least by the delays.

When looking back at the obtained results, one should recall that the considered controllers are not necessarily the architectures that provide the best performance in the presence of delays. They were merely selected as relatively simple representatives of different classes of control architectures. The goal of the comparison was not to obtain optimal controller performance, but to illustrate how the performance is compromised for each architecture to warrant stability in the presence of delays. For the P-F architecture, for example, the proportional gain K_{ps} was not altered for different delays. Consequently, the reflected stiffness was delay-independent. Lowering K_{ps} will reduce the reflected stiffness and motion tracking performance, but at the same time, the operator effort will improve because less damping is required to guarantee stability. In contrast, such a tradeoff in tuning the proportional gains is not possible for the PDd, WT, and 4C architectures, due to the high operator effort caused by K_{pm} and the delay.

We emphasize that the implemented injection of damping in free motion is not required for the P-F and PF-F architectures due to their unilateral nature. For zero injected damping, both $\Delta q_{rms}^{T_m}$ and $\tau_{h,rms}$ would be delay-independent and have a performance equal to the zero-delay case. This makes the PF-F controller a very suitable architecture for high-performance teleoperation when the communication suffers from delays. As this paper shows the potential of the direct force-reflecting PF-F controller in terms of performance, explicit stability conditions are not considered. In [10] and our related work in [14], the stability of direct force-reflecting teleoperators with delays is addressed instead. In particular, an advanced damping injection method is applied to achieve stability with minimal damping (which improves the performance in the sense of the metrics presented in this paper even further, and improves stiffness perception on impact [26]). The damping gains are increased only when stability tends to get lost (which is for the direct force-reflecting controllers typically during the impact or detachment phase of the slave with the environment), by monitoring an energy balance of the system. Alternative advanced damping injection schemes are the Time-Domain Passivity Control approach [32] or the Two-Layer approach [33]. We care to stress that those control architectures are the only ways of guaranteeing stability, whereas performance could come from one of the tested controllers in this paper. Therefore, our results are also applicable if the controllers are used in combination with one of the above-mentioned advanced damping injection methods.

Authorized licensed use limited to: ASML Netherlands B.V.. Downloaded on August 07,2020 at 07:40:17 UTC from IEEE Xplore. Restrictions apply.

VII. Conclusion

In this paper, the controller performance of six architectures is analyzed in both free motion and contact on existing metrics for motion tracking, force reflection, and stiffness reflection. The architectures are also compared on physical operator effort, which is a newly introduced metric to describe the required effort of the operator to execute free motion tasks. Four traditional bilateral motion synchronization and two direct force-reflection controllers are compared experimentally. The experimental results illustrate that, despite practical limitations such as drive-train imperfections, limited encoder resolution, and measurement noise, the overall performance improves when force sensor information is included in the controllers. The design of an architecture with position tracking terms in the master controller should be avoided to prevent a high operator effort in the presence of delays, caused by delay-induced forces. Moreover, we suggest to design a control architecture where only the slave-side controller is used for motion synchronization, and thus to control the error $q_m^{T_m} - q_s$ to zero, instead of $q_m - q_s$. Consequently, the authors believe that the direct force-reflection architectures have more potential than bilateral motion synchronization architectures when the communication suffers from delays. The direct force-reflecting PF-F architecture is affected least by the delays and, therefore, seems to be the most promising one to achieve a high performance for delayed bilateral teleoperation. Advanced damping injection methods can be exploited to increase the performance even further.

Future work encompasses the evaluation and identification of an absolute threshold for a human operator for, e.g., stiffness reflection, taking into account the fact that adding damping in free motion results in a softer perception to the operator [26]. Such a threshold indicates how high the reflected stiffness should be in order to perceive the environment as stiff. Moreover, it is interesting to develop clear metrics to quantitatively analyze the performance during the impact (i.e., the free motion to contact transition) phase, and to extend the results of this paper to teleoperation systems with multiple DOFs (see, e.g., [34, Ch. 5]).

References

[1] P. F. Hokayem and M. W. Spong, “Bilateral teleoperation: An historical survey,” *Automatica*, vol. 42, no. 12, pp. 2035–2057, Dec. 2006.

[2] E. Nuño, L. Basañez, and R. Ortega, “Passivity-based control for bilateral teleoperation: A tutorial,” *Automatica*, vol. 47, no. 3, pp. 485–495, Mar. 2011.

[3] W. R. Ferrell, “Delayed force feedback,” *Hum. Factors, J. Hum. Factors Ergonom. Soc.*, vol. 8, no. 5, pp. 449–455, 1966.

[4] L. van den Bedem, R. Hendrix, P. Rosielle, M. Steinbuch, and H. Nijmeijer, “Design of a minimally invasive surgical teleoperated master-slave system with haptic feedback,” in *Proc. IEEE Int. Conf. Mechatron. Automat.*, Aug. 2009, pp. 60–65.

[5] The Construction Index. *Excavator Controlled in Germany Digs in Korea*. Accessed: Apr. 26, 2019. [Online]. Available: https://www.theconstructionindex.co.uk/news/view/excavatorcontrolled-in-germany-digs-in-korea

[6] J. van Oosterhout, D. A. Abbink, J. F. Koning, H. Boessenkool, J. G. W. Wildenbeest, and C. J. M. Heemskerk, “Haptic shared control improves hot cell remote handling despite controller inaccuracies,” *Fusion Eng. Des.*, vol. 88, nos. 9–10, pp. 2119–2122, 2013.

[7] G. Niemeyer and J.-J.-E. Slotine, “Stable adaptive teleoperation,” *IEEE J. Oceanic Eng.*, vol. 16, no. 1, pp. 152–162, Jan. 1991.

[8] D. A. Lawrence, “Stability and transparency in bilateral teleoperation,” *IEEE Trans. Robot. Autom.*, vol. 9, no. 5, pp. 624–637, Oct. 1993.

[9] B. Willaert, B. Corteville, D. Reynaerts, H. Van Brussel, and E. B. V. Poorten, “Bounded environment passivity of the classical position-force teleoperation controller,” in *Proc. IEEE/RSJ Int. Conf. Intell. Robots Syst.*, Oct. 2009, pp. 4622–4628.

[10] D. Heck, “Delayed bilateral teleoperation: A direct force-reflecting control approach,” Ph.D. dissertation, Eindhoven Univ. Technol., Dept. Mech. Eng., Eindhoven, The Netherlands, 2015.

[11] R. Anderson and M. W. Spong, “Bilateral control of teleoperators with time delay,” *IEEE Trans. Autom. Control*, vol. 34, no. 5, pp. 494–501, May 1989.

[12] G. Niemeyer and J.-J. E. Slotine, “Telemanipulation with time delays,” *Int. J. Robot. Res.*, vol. 23, no. 9, pp. 873–890, 2004.

[13] R. W. Daniel and P. R. McAree, “Fundamental limits of performance for force reflecting teleoperation,” *Int. J. Robot. Res.*, vol. 17, no. 8, pp. 811–830, 1998.

[14] D. Heck, A. Saccon, R. Beerens, and H. Nijmeijer, “Direct force-reflecting two-layer approach for passive bilateral teleoperation with time delays,” *IEEE Trans. Robot.*, vol. 34, no. 1, pp. 194–206, Feb. 2018.

[15] Y. Yokokohji and T. Yoshikawa, “Bilateral control of master-slave manipulators for ideal kinesthetic coupling-formulation and experiment,” *IEEE Trans. Robot. Autom.*, vol. 10, no. 5, pp. 605–620, Oct. 1994.

[16] K. Hashtrudi-Zaad and S. E. Salcudean, “Analysis of control architectures for teleoperation systems with impedance/admittance master and slave manipulators,” *Int. J. Robot. Res.*, vol. 20, no. 6, pp. 419–445, 2001.

[17] P. Arcara and C. Melchiorri, “Control schemes for teleoperation with time delay: A comparative study,” *Robot. Auto. Syst.*, vol. 38, no. 1, pp. 49–64, Jan. 2002.

[18] I. Aliaga, A. Rubio, and E. Sánchez, “Experimental quantitative comparison of different control architectures for master-slave teleoperation,” *IEEE Trans. Control Syst. Technol.*, vol. 12, no. 1, pp. 2–11, Jan. 2004.

[19] A. Aziminejad, M. Tavakoli, R. V. Patel, and M. Moallem, “Transparent time-delayed bilateral teleoperation using wave variables,” *IEEE Trans. Control Syst. Technol.*, vol. 16, no. 3, pp. 548–555, May 2008.

[20] E. Rodríguez-Seda, D. Lee, and M. W. Spong, “Experimental comparison study of control architectures for bilateral teleoperators,” *IEEE Trans. Robot.*, vol. 25, no. 6, pp. 1304–1318, Dec. 2009.

[21] A. Sherman, M. Çavuşoğlu, and F. Tendick, “Comparison of teleoperator control architectures for palpation task,” in *Proc. ASME Dyn. Syst. Control Division*, vol. 2, 2000, pp. 1261–1268.

[22] R. Hendrix, “Robotically assisted eye surgery: A haptic master console,” Ph.D. dissertation, Dept. Mech. Eng., Eindhoven Univ. Technol., Eindhoven, The Netherlands, 2011.

[23] C. A. L. Martínez, R. van de Molengraft, and M. Steinbuch, “High performance teleoperation using switching robust control,” in *Proc. IEEE World Haptics Conf.*, Apr. 2013, pp. 383–388.

[24] D. Lee and M. W. Spong, “Passive bilateral teleoperation with constant time delay,” *IEEE Trans. Robot.*, vol. 22, no. 2, pp. 269–281, Apr. 2006.

[25] E. Nuño, R. Ortega, N. Barabanov, and L. Basañez, “A globally stable PD controller for bilateral teleoperators,” *IEEE Trans. Robot.*, vol. 24, no. 3, pp. 753–758, Jun. 2008.

[26] F. E. van Beek, D. J. F. Heck, H. Nijmeijer, W. M. B. Tiest, and A. M. L. Kappers, “The effect of damping on the perception of hardness,” in *Proc. IEEE World Haptics Conf.*, Jun. 2015, pp. 82–87.

[27] T. Namerikawa and H. Kawada, “Symmetric impedance matched teleoperation with position tracking,” in *Proc. 45th IEEE Conf. Decis. Control*, Dec. 2006, pp. 4496–4501.

[28] N. Chopra, M. W. Spong, R. Ortega, and N. E. Barabanov, “On tracking performance in bilateral teleoperation,” *IEEE Trans. Robot.*, vol. 22, no. 4, pp. 861–866, Aug. 2006.

[29] B. Willaert, B. Corteville, D. Reynaerts, H. Van Brussel, and E. B. V. Poorten, “Transparency trade-offs for a 3-channel controller revealed by the bounded environment passivity method,” in *Proc. 3rd Int. Conf. Adv. Comput.-Hum. Interact.*, Feb. 2010, pp. 66–72.

[30] T. L. Brooks, “Telerobotic response requirements,” in *Proc. IEEE Int. Conf. Syst., Man, Cybern. Conf.*, Nov. 1990, pp. 113–120.

[31] J. E. Colgate and J. M. Brown, “Factors affecting the Z-Width of a haptic display,” in *Proc. IEEE Int. Conf. Robot. Automat.*, May 1994, pp. 3205–3210.

Authorized licensed use limited to: ASML Netherlands B.V.. Downloaded on August 07,2020 at 07:40:17 UTC from IEEE Xplore. Restrictions apply.

[32] J.-H. Ryu and C. Preusche, “Stable bilateral control of teleoperators under time-varying communication delay: Time domain passivity approach,” in *Proc. IEEE Int. Conf. Robot. Automat.*, Apr. 2007, pp. 3508–3513.

[33] M. Franken, S. Stramigioli, S. Misra, C. Secchi, and A. Macchelli, “Bilateral telemanipulation with time delays: A two-layer approach combining passivity and transparency,” *IEEE Trans. Robot.*, vol. 27, no. 4, pp. 741–756, Aug. 2011.

[34] J. Rebelo, “Robust and transparent multi-degree-of-freedom bilateral teleoperation with time delay,” Ph.D. dissertation, Dept. Biomech. Eng., Delft Univ. Technol., Delft, The Netherlands, 2015.

Ruud Beerens received the M.Sc. degree in mechanical engineering from the Eindhoven University of Technology, Eindhoven, The Netherlands, in 2015, where he is currently pursuing the Ph.D. degree with the Department of Mechanical Engineering.

His current research interests include the nonlinear and hybrid control design for high-performance mechatronic systems and the control of bilateral teleoperation systems.

Dennis Heck received the M.Sc. and Ph.D. degrees in mechanical engineering from the Dynamics and Control Group, Eindhoven University of Technology, Eindhoven, The Netherlands, in 2011 and 2015, respectively. His Ph.D. research, which was supported by STW and part of the H-Haptics project, focused on the controller design for delayed bilateral teleoperation. His supervisors were Prof. Dr. H. Nijmeijer and Dr. A. Saccon.

Since 2015, he has been a Thermal Control Engineer in the high-tech semiconductor industry. His current research interests include the control of input non-affine Peltier elements and the control of complex underactuated and undersensed thermomechanical systems.

Alessandro Saccon received the Laurea degree *(cum laude)* in computer engineering and the Ph.D. degree in control system theory from the University of Padova, Padua, Italy, in 2002 and 2006, respectively.

Until 2009, he held a research and development position at the University of Padova in joint collaboration with Ducati Corse working on control and optimization methods for the exploration of the dynamics of racing motorcycles for virtual prototyping studies using multi-body models and numerical optimal control methods. From 2009 to 2012, he held a post-doctoral research position at the Instituto Superior TÂ^cnico, Lisbon, Portugal, sponsored by the Portuguese Science and Technology Foundation (FCT), working on motion planning, dynamics, and control of autonomous robotic vehicles. Since 2013, he has been an Assistant Professor in nonlinear control and robotics with the Department of Mechanical Engineering, Eindhoven University of Technology, Eindhoven, The Netherlands. His current interests include modeling, analysis, and control of multi-body systems, geometric mechanics, nonlinear control theory, and numerical optimal control for the exploration of trajectory space of complex and highly maneuverable nonlinear systems. Recent work has focused on the development of optimal constrained motion planning strategies for multiple autonomous robotic vehicles, robotics systems with unilateral position constraints, and control of mechanical systems subject to rigid contacts and impacts.

Dr. Saccon received the Claudio Maffezzoni Best Ph.D. Thesis Award from the Politecnico di Milano for his Ph.D. thesis.

Henk Nijmeijer (F’00) was born in 1955.

Since 2015, he has been the Scientific Director of the Dutch Institute of Systems and Control (DISC). He is currently a Full Professor with the Eindhoven University of Technology, Eindhoven, The Netherlands, where he also chairs the Dynamics and Control Group. He has published a large number of journal and conference papers and several books.

He has been an IFAC Council Member since 2011. He was a recipient of the 2015 IEEE Control Systems Technology Award and a member of the Mexican Academy of Sciences. He received the IEE Heaviside Premium in 1990. He is appointed as an Honorary Knight of the golden Feedback Loop (NTNU) in 2011. He is or was at the Editorial Board of numerous journals. He is an Editor of *Communications in Nonlinear Science and Numerical Simulations*.

Authorized licensed use limited to: ASML Netherlands B.V.. Downloaded on August 07,2020 at 07:40:17 UTC from IEEE Xplore. Restrictions apply.